AIAA JOURNAL
Vol. 31, No. 9, September 1993

Structural Modeling of Composite Beams with Induced-Strain Actuators

Ramesh Chandra* and Inderjit Chopra†
University of Maryland, College Park, Maryland 20742

This paper presents an analytical-experimental investigation on structural modeling of coupled composite beams with distributed induced-strain actuators. Analysis based on Vlasov theory is developed to include distributed piezoelectric actuators, either surface mounted or embedded. Salient features of composite open-section beam analysis, like constrained warping and transverse shear deformation, were included. Induced-strain actuation was introduced in the constitutive relations of plate segment of the open-section composite beams. To evaluate the analytical predictions, several bending-torsion and extension-torsion coupled graphite-epoxy solid beams were fabricated using an autoclave molding technique. These were surface mounted with piezoelectric actuators. The actuators were excited to produce local bending moment and axial force on the beam, and the structural response was measured in terms of bending slope, induced twist, and surface strain. Good correlation between analysis and experiment was achieved. Because of the existence of a chordwise actuator moment, the induced twist of bending-torsion coupled beams was significantly influenced by including the chordwise curvature of the plate segment of beam in the formulation. For $[45]_{24}$ solid beams, the chordwise bending of the plate segment of beam was found to increase the tip twist by about 110%.

Nomenclature

b_a, b_s	= widths of piezoelectric actuator and solid beam substructure, respectively
d_{31}	= piezoelectric coefficient; 3 refers to polarization direction and 1 refers to beam axis
$\bar{E}$	$= E_s/E_a$
E_a, E_s	= Young's moduli of actuator and substructure, respectively
E_ℓ, E_t	= Young's moduli of any ply of composite beam in ℓ and t directions, respectively
$G_{\ell t}$	= shear modulus of any ply of composite beam in ℓt plane
h	= thickness of solid beam with actuator and copper sheet ($t_s + 2t_a + 2t_c$)
K_{ij}	= stiffness matrix for beam
k_s, k_z, k_{sz}	= bending curvatures referring to plate segment of beam; $K_s = u_{,ss}$, $k_z = u_{,zz}$, $k_{sz} = 2u_{,sz}$
ℓ_a, ℓ_s	= length of actuator and substructure, respectively
M_s, M_z, M_{sz}	= moment resultants, referring to plate segment of beam
M_x, M_y	= bending moments, referring to beam
M_ω	= bimoment (or warping moment), referring to beam
N	= axial force, referring to beam
N_s, N_z, N_{sz}	= stress resultants, referring to plate segment of beam
n, s, z	= coordinate system for plate segment of beam, Fig. 1b
T	= torsion moment, referring to beam
$\bar{t}$	$= t_s/t_a$
t_a, t_s	= thicknesses of actuator and substructure, respectively
t_c	= thickness of copper sheet
U, V, W	= displacements in x, y, z directions, respectively (referring to beam)
u, v, w	= displacements in n, s, z directions, respectively (referring to plate segment of beam)
V	= applied voltage
V_x, V_y	= shear forces in x, y directions, respectively (referring to beam)
γ	$= \bar{E}\bar{t}$
x, y, z	= coordinate system for open section beam, Fig. 1a
ϵ_s, ϵ_z, ϵ_{sz}	= total strains, referring to plate segment of beam
ϵ_{xz}, ϵ_{yz}	= transverse shear strains for the beam in xz and yz planes, respectively
ϵ_s^0, ϵ_z^0, ϵ_{sz}^0	= membrane strains, referring to plate segment of beam
ϕ_x, ϕ_y, ϕ_z	= rotations about x, y, z axes, respectively (referring to beam)
λ	= warping function
μ	= constrained warping parameter, $\sqrt{(K_{55})_r/K_{44}}\,\ell$
$\mu_{\ell t}$	= Poisson's ratio of any ply of composite beam in the ℓt plane
σ_s, σ_z, σ_{sz}	= stress field, referring to plate segment of beam
$(\,)'$	= differentiation with respect to z coordinate
$(\dot{})$	= differentiation with respect to s coordinate
$[\,]^T$	= transpose

Received Sept. 5, 1992; revision received Jan. 23, 1993; accepted for publication Feb. 2, 1993.

*Assistant Research Scientist, Department of Aerospace Engineering. Senior Member AIAA.
†Professor, Department of Aerospace Engineering. Fellow AIAA.

Introduction

APPLICATION of smart structures technology to helicopter rotors appears promising to enhance rotor performance by reducing vibratory response and increasing stability. A smart structure consists of substructure with sensors, controllers, and actuators. To exploit the potential benefits of smart structures technology, it is important to develop an accurate structural modeling of the substructure with sensors, controllers, and actuators, so that its deformation characteristics under mechanical and electrical loads could be predicted. Modern helicopters are tending toward hingeless and bearingless rotors. These rotors are stiffer than articulated rotors but

are susceptible to higher vibratory loads and aeromechanical instabilities. As an example, a bearingless rotor consists of a torsionally soft open-section flexbeam at the inboard end (up to 25% radius) and a multicell main blade, normally built of composite materials. Hence, structural modeling of open-section composite beams (for flexbeam) and multicell composite blades with distributed actuators is needed. Additionally, including bending-torsion and extension-torsion couplings due to composite laminates in these substructures would further enhance the potential of smart structures in rotors.

The authors[1] developed an analytical formulation based upon Vlasov theory[2] for open-section composite beams with bending-torsion and extension-torsion couplings. The transverse shear deformation of the cross section was included. The analysis was used to predict the static structural response of coupled I beams under bending and torsional loads. The predicted results were correlated satisfactorily with experimental data for graphite-epoxy I beams. The analysis was also extended to calculate free vibration characteristics of rotating composite I beams.[3] The predicted natural frequencies and mode shapes were successfully correlated with experimental values obtained by testing the coupled composite beams in an in-vacuo rotor test facility. These studies showed the importance of constrained warping in predicting the bending-torsion behavior of open-section composite beams. The authors[4,5] further developed a composite beam analysis for closed-section beams, including multicell rotor blades with couplings. Again, the analytical predictions were successfully correlated by experiments. Feasibility of achieving a sufficient level of extension-torsion coupling for tilt rotor design was shown. These studies, though confined to the composite beams under mechanical loads, provide a basis to model induced-strain actuation.

Crawley and de Luis[6] presented an analytical-experimental study on structural modeling of composite beams of solid rectangular cross section with surface mounted or embedded distributed piezoelectric actuators. Modeling of substructure with surface mounted actuators included a shear lag effect arising due to the finite thickness of the adhesive layer between piezoelectric actuators and substructure, whereas the substructure with embedded actuators was modeled with the assumption of perfect bonding between the piezoelectric actuators and layers of the substructure. The normal strain in the actuator was assumed to be uniform across its thickness. Analytical prediction of dynamic response of cantilever composite beams with piezoelectric actuators excited by sinusoidal signals was validated by experiments. Crawley and Anderson[7] presented models describing the detailed mechanics of induced-strain actuation of beams via piezoelectric effect. Under induced-strain actuation, the beams undergo extension, bending, and localized shear deformations. To assess the importance of these modes of deformation, they calculated structural response using the uniform strain model,[6] Bernoulli-Euler model, and finite element model. Measured surface strains from substructure and actuator were used for validation of these models. The Bernoulli-Euler model was found to be more accurate than the uniform strain model. The influence of nonideal effects such as nonlinearity in field-strain relation, hysteresis, etc., was included in the analysis. Crawley et al.[8] presented piezoelectric technology for applications in the active control of smart structures. Mechanical models for the interaction of piezoactuators with one- and two-dimensional structures were derived. An electromechanical coupling model of a piezoelectric element was used to derive the optimal resistive and tuned electrical circuits to maximize the damping characteristics of the structure.

Crawley and Lazarus[9] presented an analytical-experimental study on anisotropic plates with induced-strain actuators. The analysis was based on classical laminated plate theory; Rayleigh-Ritz technique was used to provide solutions for cantilever plates, and good correlation with the experimental data was shown.

Im and Atluri[10] developed a nonlinear analytical model to examine the structural behavior of a finitely deformed beam with a piezoactuator under a general loading. In this model, axial force and transverse shear acting on the substructure were also considered. A significant influence of mechanical loading on the shear stress distribution in the adhesive layer was shown. Robbins and Reddy[11] presented a finite element analysis of actuated beams. Four different finite element models—two based on "equivalent single-layer" and two based on "multi-layer"—were developed. For better physical insight of load transfer between the actuator and substructure, the need to use an analysis with transverse shear deformation was highlighted. Results were presented for static as well as dynamic loading conditions. The multilayered shear-deformation finite element model was shown to be the most accurate in predicting stress and the displacement field.

Thus, it is seen that the studies dealing with induced-strain actuation were confined to plates and solid section beams and did not include coupled composite open section beams. Also, these analyses were restricted to beams undergoing bending and extensional deformations. The objective of the present investigation is to develop a formulation for open-section coupled composite beams, including solid section beams with distributed actuators undergoing bending and extensional and torsional deformations, and to generate experimental data to validate the analysis.

Analysis

In this investigation, Vlasov theory is used to model open-section coupled composite beams with distributed induced-strain actuators. In this analysis, two-dimensional stress and displacement fields associated with a general plate segment of the beam are reduced to one-dimensional generalized forces and displacements of the beam. The induced-strain actuators are modeled at plate segment level.

The analysis uses three coordinate systems: an orthogonal right-handed Cartesian coordinate system (x, y, z) for the beam; an orthogonal coordinate system (n, s, z) for any plate segment of the beam, where the n axis is normal to the midsurface of any plate segment, the s axis is tangential to the midsurface and is along the contour line of the beam cross section, and the z axis is along the longitudinal axis of beam, Fig. 1a; and a contour coordinate system s, where s is measured along the contour line of the cross section from a judiciously selected origin, Fig. 1b. The generalized beam forces are V_x, V_y, V_z, M_x, M_y, T, M_ω, and M_c. The torsional moment T consists of unconstrained warping torsion (Saint Venant torsion) and constrained warping torsion (Vlasov torsion). As shown later, the Vlasov torsion and bimoment M_ω are related to each other. M_c is related to the chordwise bending moment (section moment) of the plate segment of the beam. Note that the present analysis is intended for open-section composite beams, such as I, cruciform section, etc., which are built of several flat rectangular composite segments.

Kinematics

From geometric considerations, Fig. 1b, generalized beam displacements U, V, and ϕ_z are related to the displacements $u(z, s)$ and $v(z, s)$ associated with a generic plate segment of the beam as follows:

$$u(s,z) = U(z)\sin\theta(s) - V(z)\cos\theta(s) - q(s)\phi_z(z) \quad (1)$$

$$v(s,z) = U(z)\cos\theta(s) + V(z)\sin\theta(s) + r(s)\phi_z(z) \quad (2)$$

where r, q, and θ are shown in Fig. 1b.

Note that the relations (1) and (2) are in accordance with the fundamental assumption that the cross section does not deform in its plane. This assumption does not permit the bending of the plate segment of the beam in the s direction. This chordwise bending plays an important role in the prediction of

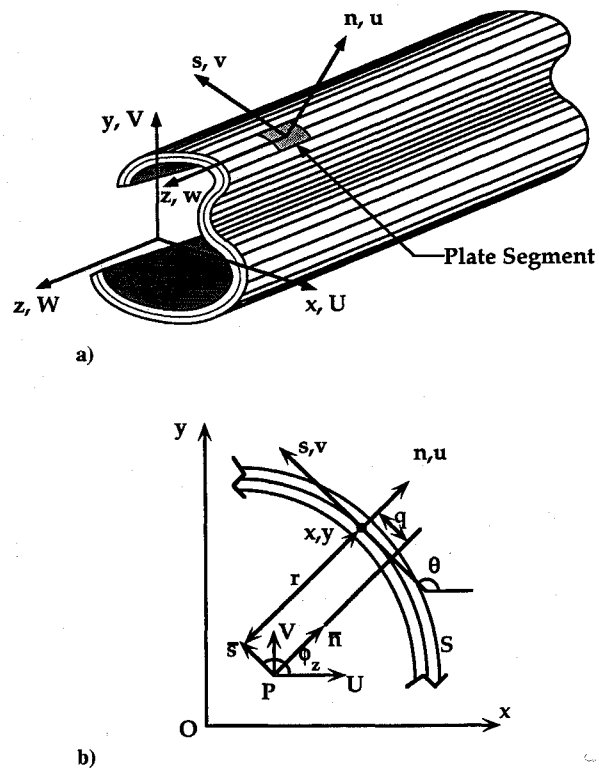

Fig. 1 a) Cartesian coordinates in open-section beam, and b) pictorial definitions of beam displacements and rotations.

torsional behavior of bending-torsion coupled plates.[12] To account for this bending, relations (1) and (2) are modified to

$$u(s,z) = U(z)\sin\theta(s) - V(z)\cos\theta(s) - q(s)\phi_z(z) - \alpha(s)\psi(z) \tag{3}$$

$$v(s,z) = U(z)\cos\theta(s) + V(z)\sin\theta(s) + r(s)\phi_z(z) \tag{4}$$

where $\psi(z)$ represents chordwise curvature of the plate segment and $\alpha(s)$ is given in the Appendix. The other inplane displacement $w(z, s)$ associated with the plate segment is determined from the following strain-displacement relation:

$$\epsilon^0_{zs} = \dot{w} + v' \tag{5}$$

The inplane shear strain ϵ^0_{sz} depends upon transverse shear strains of the beam and is related by the following equation:

$$\epsilon^0_{zs} = \epsilon_{xz}\cos\theta + \epsilon_{yz}\sin\theta \tag{6}$$

Using relations (4–6), $w(z, s)$ is obtained as:

$$w = W + x\phi_x + y\phi_y - \lambda\phi'_z \tag{7}$$

where λ is expressed in terms of sectorial area as

$$\lambda = \int_s r\,ds$$

and

$$\phi_x = \epsilon_{xz} - U' \qquad \phi_y = \epsilon_{yz} - V' \tag{8}$$

Relations (3), (4), and (7) provide the connection between one-dimensional generalized beam displacements and two-dimensional displacements associated with a generic plate segment of the beam.

Membrane strain associated with a generic plate segment ϵ^0_z and ϵ^0_s are related by the following equations:

$$\epsilon^0_z = w' \tag{9}$$

$$\epsilon^0_s = \dot{v} \tag{10}$$

Using relations (4), (7), (9), and (10), ϵ^0_z and ϵ^0_s are obtained as

$$\epsilon^0_z = W' + x\phi'_x + y\phi'_y - \lambda\phi''_z \tag{11}$$

$$\epsilon^0_s = (-U\sin\theta + V\cos\theta)\dot{\theta} + \dot{r}\phi_z \tag{12}$$

Similarly, k_z and k_{zs} are obtained as

$$k_z = -\sin\theta\phi'_x + \cos\theta\phi'_y - q\phi''_z + \epsilon'_{xz}\sin\theta - \epsilon'_{yz}\cos\theta - \alpha\psi'' \tag{13}$$

$$k_s = -\ddot{\alpha}\psi \tag{14}$$

$$k_{zs} = -2(\phi'_z + \dot{\alpha}\psi') \tag{15}$$

Modeling of Induced-Strain Actuation

The strain field develops in a piezoelectric actuator when an electric voltage is applied across its faces. The induced-strain field for a free piezoelectric actuator is

$$\epsilon^{(a)}_z = d_{31}(V/t_a) \qquad \epsilon^{(a)}_s = d_{31}(V/t_a) \qquad \epsilon^{(a)}_{sz} = 0 \tag{16}$$

Using classical plate theory, the strain field in the plate segment of the actuated beam is

$$\{\epsilon\} = \{\epsilon^0\} + n\{k\} \tag{17}$$

The constitutive relation for any ply of the plate segment with actuator is

$$\{\sigma\} = [\bar{Q}](\{\epsilon\} - \{\epsilon^{(a)}\}) \tag{18}$$

where

$$\{\sigma\} = \{\sigma_s \quad \sigma_z \quad \sigma_{sz}\}^T; \qquad \{\epsilon\} = \{\epsilon_s \quad \epsilon_z \quad \epsilon_{sz}\}^T$$

$$\{\epsilon^{(a)}\} = \{\epsilon^{(a)}_s \quad \epsilon^{(a)}_z \quad \epsilon^{(a)}_{sz}\}^T$$

The actuation strain vector $\{\epsilon^{(a)}\}$ for a piezoelectric actuator, which contains inplane normal strain components and no shear strain component, manifests itself in the formulation similar to the thermal strain. The consistent plate relations in terms of stress and moment resultants are obtained by substituting the assumed strain relation into the constitutive relation and integrating through the thickness of the plate segment as

$$\begin{Bmatrix} N \\ M \end{Bmatrix} = \begin{bmatrix} A & B \\ B & D \end{bmatrix} \begin{Bmatrix} \epsilon^0 \\ k \end{Bmatrix} - \begin{Bmatrix} N^{(a)} \\ M^{(a)} \end{Bmatrix} \tag{19}$$

where

$$\{N\} = \{N_s \quad N_z \quad N_{sz}\}^T; \qquad \{M\} = \{M_s \quad M_z \quad M_{sz}\}^T$$

$$\{\epsilon^0\} = \{\epsilon^0_s \quad \epsilon^0_z \quad \epsilon^0_{sz}\}^T$$

$$\{k\} = \{k_s \quad k_z \quad k_{sz}\}^T; \qquad \{N^{(a)}\} = \int_h [\bar{Q}]\{\epsilon^{(a)}\}\,dn$$

$$\{M^{(a)}\} = \int_h [\bar{Q}]\{\epsilon^{(a)}\}n\,dn \tag{20}$$

Note that the A, B, and D matrices depend on substructure and actuators, whereas $\{N^{(a)}\}$ and $\{M^{(a)}\}$ depend only on actuator plies.

Specializing the generalized actuation forces for a bending actuator (two piezoelectric elements with substructure in be-

tween are configured in such a way that one creates tensile strain whereas the other creates compressive strain under an applied electric field):

$$N_z^{(a)} = 0; \qquad N_s^{(a)} = 0; \qquad N_{sz}^{(a)} = 0$$

$$M_z^{(a)} = \int_h (\bar{Q}_{11} + \bar{Q}_{12})\Lambda n \, dn \tag{21}$$

$$M_s^{(a)} = \int_h (\bar{Q}_{12} + \bar{Q}_{22})\Lambda n \, dn; \qquad M_{sz}^{(a)} = 0$$

where $\Lambda = V(d_{31}/t_a)$.

Relations (19) are rewritten as

$$\begin{aligned}
N_z &= A_{11}\epsilon_z + A_{12}\epsilon_s + A_{16}\epsilon_{zs} + B_{11}k_z + B_{12}k_s \\
&\quad + B_{16}k_{zs} - N_z^{(a)} \\
N_s &= A_{12}\epsilon_z + A_{22}\epsilon_s + A_{26}\epsilon_{zs} + B_{12}k_z + B_{22}k_s \\
&\quad + B_{26}k_{zs} - N_s^{(a)} \\
N_{zs} &= A_{16}\epsilon_z + A_{26}\epsilon_s + A_{66}\epsilon_{zs} + B_{16}k_z + B_{26}k_s + B_{66}k_{zs} \\
M_z &= B_{11}\epsilon_z + B_{12}\epsilon_s + B_{16}\epsilon_{zs} + D_{11}k_z + D_{12}k_s \\
&\quad + D_{16}k_{zs} - M_z^{(a)} \\
M_s &= B_{12}\epsilon_z + B_{22}\epsilon_s + B_{26}\epsilon_{zs} + D_{12}k_z + D_{22}k_s \\
&\quad + D_{26}k_{zs} - M_s^{(a)} \\
M_{zs} &= B_{16}\epsilon_z + B_{26}\epsilon_s + B_{66}\epsilon_{zs} + D_{16}k_z + D_{26}k_s + D_{66}k_{zs}
\end{aligned} \tag{22}$$

where $[A]$, $[B]$, and $[D]$ refer to laminate stiffnesses.[1] The stress and moment resultants due to bending actuation are obtained from relation (21). It is to be noted that ϵ_s, k_s, N_s, and M_s appear in the relations (22) due to the bending in the s direction.

Bar Forces and Their Equilibrium Equations

The generalized bar forces and their equilibrium equations are derived by applying the principle of virtual work.[2] The external work done by the plate forces during a virtual displacement of the cross section is:

$$W_e = \int_s [N_z w + N_s v + N_{zs} v + M_z u' + M_s \dot{u} - Q_z u - M_{zs}\phi_z] \, ds + \sum_{\text{branches}} (M_{zs}^j u^j - M_{zs}^i u^i) \tag{23}$$

Note that N_s and M_s, representing the chordwise stress and moment resultants, are included in the preceding relation. The second term in Eq. (23) refers to the contribution in the work done by concentrated forces acting in the cross section.

From relation (3),

$$\dot{u} = (U\cos\theta + V\sin\theta)\dot{\theta} - \dot{q}\phi_z - \dot{\alpha}\psi \tag{24}$$

From Ref. 2,

$$\dot{\theta} = 1/a \qquad \text{and} \qquad \dot{q} = 1 - (r/a) \tag{25}$$

where a is the radius of curvature of the branches of the beam. For beams with flat branches, a is infinite. Hence,

$$\dot{\theta} = 0 \qquad \text{and} \qquad \dot{q} = 1 \tag{26}$$

Introducing relations (26) in relation (24)

$$\dot{u} = -\phi_z - \dot{\alpha}\psi \tag{27}$$

Using relations (3), (4), and (7) and taking the variation of W_e,

$$\delta W_e = N\delta W + V_x\delta U + V_y\delta V + T\delta\phi_z + M_\omega\delta\phi_z' + M_y\delta\phi_x + M_x\delta\phi_y + F_x\delta\epsilon_{xz} + F_y\delta\epsilon_{yz} + H\delta\psi + I\delta\psi' \tag{28}$$

where

$$N = \int_s N_z \, ds - N^{(a)} \tag{29}$$

$$V_x = \int_s (N_{zs}\cos\theta + N_s\cos\theta - Q_z\sin\theta) \, ds + \sum_{\text{branches}} (M_{zs}^j\sin\theta^j - M_{zs}^i\sin\theta^i) - V_x^{(a)} \tag{30}$$

$$V_y = \int_s (N_{zs}\sin\theta + N_s\sin\theta + Q_z\cos\theta) \, ds + \sum_{\text{branches}} (-M_{zs}^j\sin\theta^j + M_{zs}^i\sin\theta^i) - V_y^{(a)} \tag{31}$$

$$T = \int_s (N_{zs}r + N_s r - M_{zs} - M_s + Q_z q) \, ds + \sum_{\text{branches}} (-M_{zs}^j q^j - M_{zs}^i q^i) \tag{32}$$

$$M_\omega = -\int_s (N_z\lambda + M_z q) \, ds \tag{33}$$

$$M_x = \int_s (N_z y + M_z\cos\theta) \, ds - M_x^{(a)} \tag{34}$$

$$M_y = \int_s (N_z x + M_z\sin\theta) \, ds - M_y^{(a)} \tag{35}$$

$$F_x = \int_s M_z\sin\theta \, ds - F_x^{(a)} \tag{36}$$

$$F_y = -\int_s M_z\cos\theta \, ds + F_y^{(a)} \tag{37}$$

$$H = \int_s (-\dot{\alpha}M_s + \alpha Q_z) \, ds + \sum_{\text{branches}} (M_{zs}^j\alpha^j - M_{zs}^i\alpha^i) - H^{(a)} \tag{38}$$

$$I = \int_s M_z\alpha \, ds + I^{(a)} \tag{39}$$

where generalized forces due to actuation are

$$\begin{aligned}
N^{(a)} &= \int_s N_z^{(a)} \, ds \\
V_x^{(a)} &= \int_s N_s^{(a)}\cos\theta \, ds \\
V_y^{(a)} &= \int_s N_s^{(a)}\sin\theta \, ds \\
M_x^{(a)} &= \int_s (N_z^{(a)} y + M_z^{(a)}\cos\theta) \, ds \\
M_y^{(a)} &= \int_s (N_z^{(a)} x - M_z^{(a)}\cos\theta) \, ds \\
F_x^{(a)} &= \int_s M_z^{(a)}\cos\theta \, ds \\
F_y^{(a)} &= \int_s M_z^{(a)}\cos\theta \, ds
\end{aligned} \tag{40}$$

$$H^{(a)} = \int_s M_s^{(a)} \dot{\alpha}\, ds$$

$$I^{(a)} = \int_s M_z^{(a)} \alpha\, ds$$

It is difficult to compute the generalized bar forces V_x, V_y, and T from relations (30), (31), and (32) because of the contributions from different branches. These are simplified by using equilibrium equations of plate forces[2]

$$V_x = -M_y' \tag{41}$$

$$V_y = M_x' \tag{42}$$

$$T = T_s + T_\omega \tag{43}$$

where T_s is Saint Venant torsion (free warping) and T_ω is Vlasov torsion (constrained warping). These are defined as:

$$T_s = -2\int_s (M_{sz} + M_s)\, ds \tag{44}$$

$$T_\omega = \int_s (N_{zs} r + M_z' q)\, ds \tag{45}$$

By using the plate equilibrium equation, relation (45) is simplified to

$$T_\omega = -M_\omega' \tag{46}$$

This gives the relationship between Vlasov torsion and warping moment (or bimoment).

The external work done by the applied loadings on the plate segment of the beam in a virtual displacement of the cross section is

$$W_e = n\delta W + v_x \delta U + v_y \delta V + t\delta\phi_z + m_\omega \delta\phi_z' + m_y \delta\phi_x + m_x \delta\phi_y + f_x \delta\epsilon_{xz} + f_y \delta\epsilon_{yz} + m_h \delta\psi + i_\omega \delta\psi' \tag{47}$$

where n, v_x, v_y, t, m_ω, m_y, m_x, f_x, f_y, m_h, and i_ω are generalized load intensities on the beam, derived from the loadings on plate segment.[2] The strain energy Π is given as

$$\Pi = \frac{1}{2}\int_s (N_z \epsilon_z + N_s \epsilon_s + N_{zs}\epsilon_{zs} + M_z k_z + M_s k_s + M_{zs} k_{zs})\, ds \tag{48}$$

Using the relations between bar forces and plate forces, the strain energy becomes

$$\Pi = \frac{1}{2}\int_s [NW' + M_y\phi_x' + M_x\phi_y' + T\phi_z' + M_\omega\phi_z'' + F_x\epsilon_{xz}' + F_y\epsilon_{yz}' + G_x\epsilon_{xz} + G_y\epsilon_{yz} + M_c\psi + M_h\psi' + I_\omega\psi'']\, ds \tag{49}$$

The internal virtual work W_i is obtained from the strain energy as

$$-W_i = NW' + M_y\phi_x' + M_x\phi_y' + T\phi_z' + M_\omega\phi_z'' + F_x\epsilon_{xz}' + F_y\epsilon_{yz}' + G_x\epsilon_{xz} + G_y\epsilon_{yz} + M_c\psi + M_h\psi' + I_\omega\psi'' \tag{50}$$

where

$$G_x = \int_s N_{zs}\cos\theta\, ds \tag{51}$$

$$G_y = \int_s N_{zs}\sin\theta\, ds \tag{52}$$

$$M_c = -\int_s M_s\ddot{\alpha}\, ds \tag{53}$$

$$M_h = -2\int_s \dot{\alpha} M_{zs}\, ds \tag{54}$$

$$I_\omega = -\int_s \alpha M_z\, ds \tag{55}$$

Equilibrium equations for bar forces are obtained by considering a bar element and equating the external work to internal work for any virtual displacement. Thus, seven independent equations with seven generalized displacements (U, V, W, ϕ_x, ϕ_y, ϕ_z, and ψ) as variables can be obtained. From the force-displacement relations, several interesting cases can be examined. Using the beam forces-plate forces relations, the plate constitutive relations, and the plate strain-beam displacement relations, the relations between generalized beam forces and displacements are obtained as

$$\begin{bmatrix} N-N^{(a)} \\ M_x-M_x^{(a)} \\ -M_y+M_y^{(a)} \\ M_\omega \\ T_s \\ G_x \\ G_y \\ F_x-F_x^{(a)} \\ F_y-F_y^{(a)} \\ M_c-M_c^{(a)} \\ I \end{bmatrix} = \begin{bmatrix} K_{11} & K_{12} & K_{13} & K_{14} & K_{15} & K_{16} & K_{17} & K_{18} & K_{19} & K_{110} & K_{111} \\ & K_{22} & K_{23} & K_{24} & K_{25} & K_{26} & K_{27} & K_{28} & K_{29} & K_{210} & K_{211} \\ & & K_{33} & K_{34} & K_{35} & K_{36} & K_{37} & K_{38} & K_{39} & K_{310} & K_{311} \\ & & & K_{44} & K_{45} & K_{46} & K_{47} & K_{48} & K_{49} & K_{410} & K_{411} \\ & & & & K_{55} & K_{56} & K_{57} & K_{58} & K_{59} & K_{510} & K_{511} \\ & & & & & K_{66} & K_{67} & K_{68} & K_{69} & K_{610} & K_{611} \\ & & & & & & K_{77} & K_{78} & K_{79} & K_{710} & K_{711} \\ & & & \text{symmetric} & & & & K_{88} & K_{89} & K_{810} & K_{811} \\ & & & & & & & & K_{99} & K_{910} & K_{911} \\ & & & & & & & & & K_{1010} & K_{1011} \\ & & & & & & & & & & K_{1111} \end{bmatrix} \begin{bmatrix} W' \\ \phi_y' \\ \phi_x' \\ \phi_z'' \\ \phi_z' \\ \epsilon_{xz} \\ \epsilon_{yz} \\ \epsilon_{xz}' \\ \epsilon_{yz}' \\ \psi \\ \psi' \end{bmatrix} \tag{56}$$

The analysis is sufficiently general to predict the structural response of any open-section composite beam. Using the force-displacement relations (56) and following the procedure given in Ref. 1, the bending slope and induced twist in a bending-torsion coupled composite I beam under piezoactuation are

$$V' = M_x^{(a)}\left[\frac{z}{K_{22}} + \left(\frac{K_{25}}{K_{22}}\right)^2 \frac{\ell}{\mu(K_{55})_r}\left\{\frac{\mu}{\ell}z - \sinh\frac{\mu}{\ell}z + \tanh\mu\left(\cosh\frac{\mu}{\ell}z - 1\right)\right\}\right]$$
$$\phi_z = \frac{T_e\ell}{\mu(K_{55})_r}\left[\frac{\mu}{\ell}z - \sinh\frac{\mu}{\ell}z + \tanh\mu\left(\cosh\frac{\mu}{\ell}z - 1\right)\right] \tag{57}$$

where

$$T_e = \frac{K_{25}K_{1010} - K_{510}K_{210}}{K_{22}K_{1010} - K_{210}^2}M_x^{(a)} + \frac{K_{22}K_{510} - K_{25}K_{210}}{K_{22}K_{1010} - K_{210}^2}M_c^{(a)}$$
$$(K_{55})_r = K_{55} + \frac{K_{510}^2K_{22} + K_{25}^2K_{1010}}{K_{210}^2 - K_{1010} - K_{22}}$$

These results are specialized for the free warping torsion case as

$$V' = M_x^{(a)}z\left[\frac{1}{K_{22}} + \left(\frac{K_{25}}{K_{22}}\right)^2\frac{1}{(K_{55})_r}\right]$$
$$\phi_z = T_e z\left(\frac{K_{25}}{K_{22}}\right)\frac{1}{(K_{55})_r} \tag{58}$$

As the magnitude of induced force/moment due to the state-of-art piezoceramic device is low, the experimental evaluation of the analysis needs flexible beams. It is relatively easy to design flexible beams of solid rectangular sections rather than of I or cruciform sections. Hence, this analysis is experimentally evaluated for bending-torsion and extension-torsion coupled composite beams of solid rectangular cross section; however, analytical results for bending-torsion coupled composite I beams are also presented.

Bending-Torsion Coupled Solid Beams

The bending-torsion coupling can be created in open-section composite beams using angle plies. In solid rectangular section beams, angle ply layup with midplane symmetry results in bending-torsion coupling. The force-displacement relations for these beams become

$$\begin{Bmatrix} N \\ G_x \\ G_y \end{Bmatrix} = \begin{bmatrix} K_{11} & K_{16} & K_{17} \\ K_{16} & K_{66} & 0 \\ K_{17} & 0 & K_{77} \end{bmatrix}\begin{Bmatrix} W' \\ \epsilon_{xz} \\ \epsilon_{yz} \end{Bmatrix} \tag{59}$$

$$\begin{Bmatrix} M_x - M_x^{(a)} \\ T_s \\ M_c - M_c^{(a)} \end{Bmatrix} = \begin{bmatrix} K_{22} & K_{25} & K_{210} \\ K_{25} & K_{55} & K_{510} \\ K_{210} & K_{510} & K_{1010} \end{bmatrix}\begin{Bmatrix} \phi_y' \\ \phi_x' \\ \psi \end{Bmatrix} \tag{60}$$

$$M_\omega = K_{44}\phi_z'' \tag{61}$$

where the elements of the $[K]$ matrix are given in the Appendix.

Note that the effects of constrained warping and direct transverse shear are not significant for these solid beams and, hence, are neglected.[13] The structural response of these beams under a bending actuator is obtained from relations (60) as follows:

$$V' = -\int_0^z (L_{22}M_x^{(a)} + L_{210}M_c^{(a)})\,dz$$
$$\phi_z = -\int_0^z (L_{25}M_x^{(a)} + L_{510}M_c^{(a)})\,dz \tag{62}$$

where

$$[L] = [K]^{-1} \tag{63}$$

The beam bending moments due to piezoelectric actuation $M_x^{(a)}$ and $M_c^{(a)}$ are obtained from relations (40) and (53).

$$M_x^{(a)} = b_a M_z^{(a)} \qquad M_c^{(a)} = b_a M_s^{(a)} \tag{64}$$

The bending moments due to piezoelectric actuation associated with the plate segment $M_z^{(a)}$ and $M_s^{(a)}$ are obtained from relation (21).

$$M_z^{(a)} = M_s^{(a)} = \frac{E_a}{1-\mu_a}\Lambda t_a(h - t_a) \tag{65}$$

This checks with the expression given by Crawley et al.[8]

Using relations (60) without chordwise bending, bending slope and surface strain in an isotropic beam with a bending actuator are obtained as

$$V' = \frac{1}{K_{22}}b_a\frac{E_a}{1-\mu_a}\Lambda t_a(h - t_a)\,\ell_a \tag{66}$$

$$\epsilon_z = \frac{1}{K_{22}}b_a\frac{E_a}{1-\mu_a}\Lambda t_a(h - t_a)\frac{h}{2} \tag{67}$$

where K_{22} represents the bending stiffness of the substructure and actuator. Substituting K_{22} from relation (A3) (see Appendix), relation (67) can be written as

$$\epsilon_z = \frac{6(1 + t_a/t_s)(2/t_s)\Lambda}{6 + E_s t_s/E_a t_a + 12(t_a/t_s) + (t_a/t_s)^2}(t_s/2 + t_a) \tag{68}$$

Relation (68) checks with the expression given by Crawley and Anderson.[7]

Extension-Torsion Coupled Solid Beams

The extension-torsion coupling in an open-section beam can be created using angle plies. For solid rectangular-section composite beams, antisymmetric ply layup results in extension-torsion coupling. The force-displacement relations for these beams become

$$\begin{bmatrix} N - N^{(a)} \\ T_s \end{bmatrix} = \begin{bmatrix} K_{11} & K_{15} \\ K_{15} & K_{55} \end{bmatrix}\begin{Bmatrix} W' \\ \phi_z' \end{Bmatrix} \tag{69}$$

$$M_\omega = K_{44}\phi_z'' \tag{70}$$

$$\begin{bmatrix} M_x - M_x^{(a)} \\ G_x \end{bmatrix} = \begin{bmatrix} K_{22} & K_{26} \\ K_{26} & K_{66} \end{bmatrix}\begin{Bmatrix} \phi_y' \\ \epsilon_{xz} \end{Bmatrix} \tag{71}$$

$$\begin{bmatrix} -M_y + M_y^{(a)} \\ G_y \end{bmatrix} = \begin{bmatrix} K_{33} & K_{37} \\ K_{37} & K_{77} \end{bmatrix}\begin{Bmatrix} \phi_x' \\ \epsilon_{yz} \end{Bmatrix} \tag{72}$$

Tip twist in extension-torsion coupled solid beams under axial force, induced by piezoactuation, is obtained using relations (69) and (70):

$$\phi_z = \frac{K_{15}}{K_{11}K_{55} - K_{15}^2}N^{(a)}\,\ell_a\left(1 - \frac{2}{\mu}\tanh\frac{\mu}{2}\right) \tag{73}$$

Tip bending slope in these solid beams under bending moment due to piezoactuation is obtained using relation (71)

$$\phi_y = \frac{M_x^{(a)}}{K_{22} - (K_{26}^2/K_{66})}\,\ell_a \tag{74}$$

Note that the influence of direct transverse shear on bending slope is neglected in the preceding derivation; however, the influence of transverse shear-related coupling is retained.

Experiment

To provide experimental correlation to the present analysis, graphite-epoxy beams of solid rectangular cross section were built and tested under induced-strain actuation using piezoceramic elements. The beams were fabricated using an autoclave molding technique. Metal molds with spacers were used to avoid slipping of plies during curing under pressure. Peel ply was wrapped to provide the surface finish for the beam. To bleed out excess resin and to permit the escape of volatiles during the curing process, a number of bleeder and breather layers were used. A caul plate was used to facilitate the application of uniform pressure on the laminate. The layup was cured in a microprocessor-controlled autoclave according to the curing cycle provided by the manufacturer (see Ref. 5 for more fabrication details). Table 1 shows the details of bending-torsion and extension-torsion coupled composite solid beams with different ply orientations built using this process. Note that the $\pm\theta$ layup for extension-torsion coupled solid beams causes excessive induced twist due to curing temperatures. Hence, a hygrothermally stable layup[14] was used to minimize induced twist during manufacturing. A hygrothermally stable layup refers to a layup where stress resultant in the axial direction due to the curing stresses is zero but the extension-twist coupling is nonzero.

After the beams were built, piezoelectric actuators were surface-mounted on each beam. Figure 2 shows the schematic of a cantilever beam with a pair of actuators. It is important to note that a copper sheet (thickness = 0.005 in.) which is conducting on one side and insulating on the other is used to insulate the piezoactuator from the substructure and to facilitate electrical connection to the bonded side of the actuator. The structural response of these beams was measured in terms of bending slope, twist, and surface strain. The beam's bending slope and twist at any spanwise station of the beam were measured using a laser optical system. A light beam from

Table 1 Details of graphite-epoxy solid beams and PZT piezoactuator

Graphite-epoxy solid beams
Geometry: Width = 1 in. (25.4 mm), length = 36 in. (914.4 mm), thickness = 0.11 in. (2.79 mm) Clamped length = 6 in. (152.4 mm)
Properties: $E_\ell = 20.59 \times 10^6$ psi (141.9 GPa), $E_t = 1.42 \times 10^6$ psi (9.79 GPa), $G_{\ell t} = 0.87 \times 10^6$ psi (6.0 GPa), $\mu_{\ell t} = 0.42$
Bending-torsion coupled beams Layup: $[\theta]_{24}$, $\theta = 0, 15, 30, 45$
Extension-torsion coupled beams Layup: $[30]_3/[-60]_6/[30]_3/[-30]_3/[60]_6/[-30]_3$
Details of PZT piezoactuator
Geometry: Width = 1 in. (25.4 mm), length = 2 in. (50.8 mm), thickness = 0.010 in. (0.254 mm)
Mechanical properties: $E_\ell = 7 \times 10^6$ psi (48.3 GPa), $E_t = 7 \times 10^6$ psi (48.3 GPa), $G_{\ell t} = 2.73 \times 10^6$ psi (18.8 GPa), $\mu_{\ell t} = 0.3$
Induced-strain at 150 V in a free PZT material (Fig. 3) = 240 micro strain

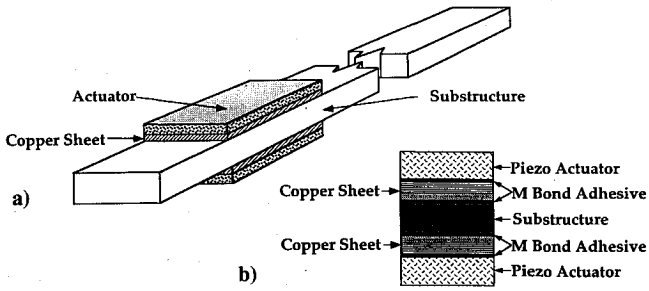

Fig. 2 a) Solid beam with piezoceramic actuators, and b) details of actuator and substructure.

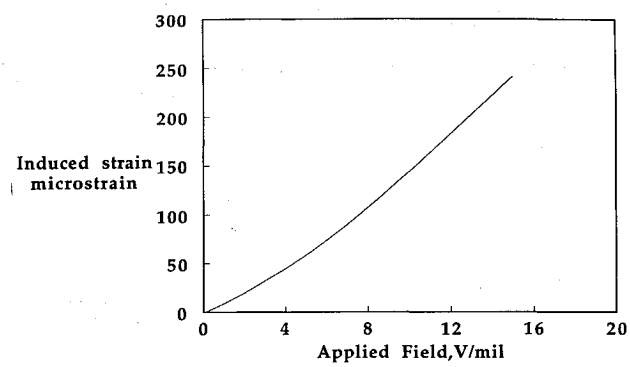

Fig. 3 Induced strain vs applied voltage curve of PZT 1195 piezoceramic actuator of 10-mil thickness.

2-m/W He-Ne laser is reflected from mirrors attached on the surface of the beam onto a vertical screen. The rotations of mirror in two orthogonal planes were obtained by measuring the movements of laser dot in two directions on the screen. To reduce the measurement error, laser-dot deflections of the order of 10 in. (254 mm) over a distance of 282 in. (7163 mm) were used. The surface strains were measured using strain gauges.

Results and Discussion

The static structural response of a solid beam under piezoactuation depends on the electromechanical characteristics of the actuator, mechanical coupling between the actuator and substructure, and the stiffness characteristics of the substructure. Mechanical coupling between the actuator and the substructure is controlled by the stiffness properties of the adhesive. In this study, the structural response is obtained for an actuator with known electromechanical properties. The induced strain produced by the actuator is used as input. Structural modeling is based on the assumption that there is a perfect bond between the actuator and the substructure. Several cases with different ply angle and thickness of the substructure are examined. Table 1 shows the details of the piezoactuators.

To create a local bending moment or an axial force, two single-layer piezoelectric elements were surface mounted on either surface of the cantilevered beam near the root end and aligned along the beam axis. To create a local bending moment, these two elements were electrically connected to produce tensile and compressive strains on opposite surfaces, whereas to generate an axial force, both were electrically connected to produce tensile or compressive strains. As the adhesive used was of high stiffness and thin bond line, a perfect bonding condition between the actuator and the substructure was assumed.

Figure 3 shows the variation of induced-strain with applied electric field in a free piezoelectric element of 10 mil (0.254 mm) thickness (PZT 1195). The thickness of the piezoceramic element was measured at several points and the average value was close to 10 mil. This curve was generated using six data

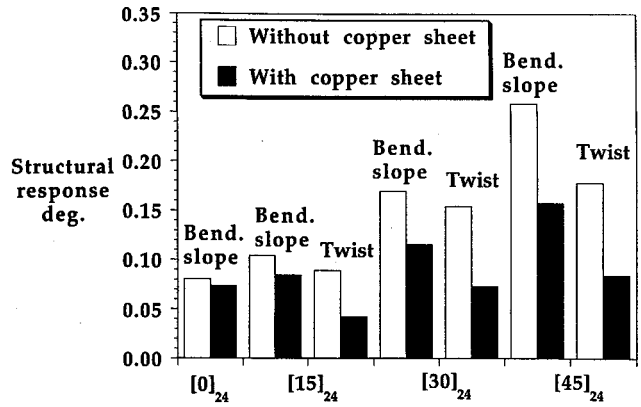

Fig. 4 Influence of copper sheet on structural response of graphite-epoxy solid beams under bending piezoactuation, applied electric field = 15 V/mil.

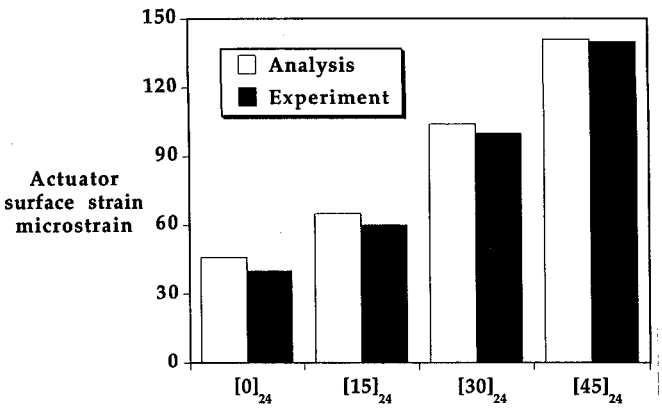

Fig. 5 Actuator surface strain for bending-torsion coupled graphite-epoxy solid beams with bending piezoactuation, applied electric field = 15 V/mil.

sets; the piezoelectric elements were initialized to zero induced strain after each test. This figure was used to provide the induced strain at an applied electric field to predict the structural response of beams under piezoactuation. Thus the induced strain of 240 micro strain at an applied field of 15 V/mil was taken from this figure and used as input for analysis.

Special copper sheet (conducting on one side and insulating on the other side) was used to insulate the substructure from piezoceramic elements and to facilitate electrical connection. This sheet placed in between the substructure and actuator reduces the effectiveness of piezoactuation of beams. The influence of this copper sheet on predicted structural response of graphite-epoxy solid beam is shown in Fig. 4. The reduction in the effectiveness of the actuator is controlled by ply angle of the beam. For $[45]_{24}$ beam, the reduction is about 50%. It is worth mentioning here that the electrical connections and conducting of the test without the copper sheet pose problems and must be carried out with utmost care.

The actuator surface strain, which is a measure of efficiency of load transfer from actuator to the substructure, depends on the stiffness ratio of substructure to actuator, shear stiffness of adhesive layer, and free actuator strain. Figure 5 shows the actuator surface strain for bending-torsion coupled graphite-epoxy solid beams with applied electric field of 15 V/mil. The free actuator strain at this field as obtained from Fig. 3 of 240 micro strain is used. One pair of piezoceramic actuators is surface mounted near the clamped end of the beam. The details of beams and actuators are given in Table 1. It is to be noted that the copper sheet was not used for these cases and actuators were mounted in such a way that both of their surfaces were accessible for electrical connections. The beams were insulated from the clamps using glass epoxy spacers. Note a higher level of strain for $[45]_{24}$ solid beam. This is due to the decrease in bending stiffness of the beam substructure with the increase in ply angle. Better correlation between theory and experiment is seen for softer beams than stiff beams. This may be due to the fact that the free actuator strain (240 micro strain) becomes smaller for constrained piezoceramic elements (see Ref. 9).

The structural response of these bending-torsion coupled graphite-epoxy beams under piezoactuation was obtained in terms of tip bending slope and twist. Figures 6 and 7 show the predicted and measured tip bending slope and twist, respectively. Note again the increase in response with the increase in ply angle. The chordwise bending of plate segment of the beam does not influence tip bending slope significantly. It is interesting to note that the chordwise bending of plate segment of beam influences the twist of these beams significantly. This is due to the existence of an actuated moment in the chordwise direction of plate segment of beam. Good correlation between analysis and experiment is achieved only when chordwise bending is included.

The structural response of coupled composite beams under multiple actuators was examined. Ten bending actuators were surface mounted on bending-torsion coupled graphite epoxy solid beams. These actuators were uniformly distributed along the length of the beams. Copper sheet in between the piezo-actuators and substructure was used for these beams. Figures 8 and 9 show the predicted and measured structural response of $[30]_{24}$ and $[45]_{24}$ beams, respectively. Note that the results given by relations (62) refer to one bending actuator. These are used to predict the structural response of solid beams subjected to bending moments created by distributed bending actuators along the span of the beam using superposition. The number of actuators referred to in these figures implies the number of actuators starting from the root which were activated. Good correlation between theory and experiment is achieved for these cases.

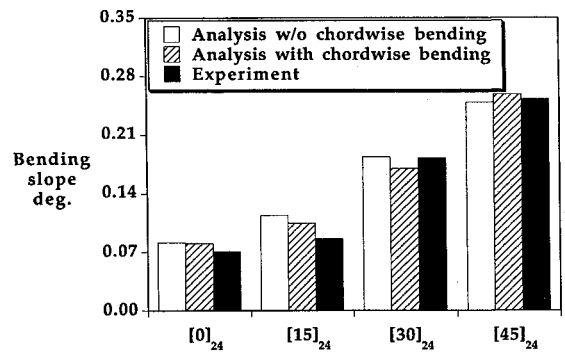

Fig. 6 Bending slope of bending-torsion coupled graphite-epoxy solid beams under bending piezoactuation, applied electric field = 15 V/mil.

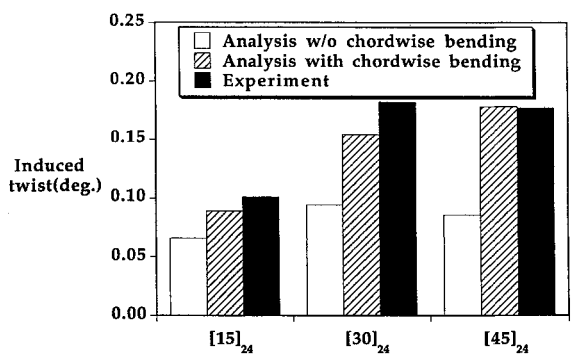

Fig. 7 Induced twist of bending-torsion coupled graphite-epoxy solid beams under bending piezoactuation, applied electric field = 15 V/mil.

To illustrate the structural behavior of extension-torsion coupled beams under piezoactuation, a solid beam with hygrothermally stable layup was examined. Fourteen piezoactuators (with 7 on each surface of the solid beam) were surface-bonded. These actuators were electrically connected to provide axial force or bending moment. The structural response of this beam under bending actuation results in pure bending, whereas the axial force due to piezoactuation causes twisting of the beam. Figure 10 shows induced bending slope and twist at the tip caused, respectively, by these two actuations. Note that the order of twist created by piezo-induced axial force is much smaller than the bending slope created by piezo-induced bending moment. Here again, good correlation between theory and experiment is achieved.

To illustrate the influence of warping constraints on structural response of open-section composite beams under piezoactuation, a bending-torsion coupled graphite-epoxy I beam was examined analytically. One bending actuator consisting of two piezoelements surface mounted on opposite flanges of an I beam was placed near the root of the beam. This bending actuator applied local bending moments; and, due to bending-torsion coupling, caused bending and twisting of this beam. Figure 11 shows the results in terms of tip bending slope and twist of this beam. Relations (57) and (58) were used to calculate the results with and without constrained warping effects, respectively. Warping constraints increase the torsional stiffness of the beam, and this increase is controlled by the constrained warping parameter μ (see Ref. 1). This parameter, in turn, depends on the stiffnesses $(K_{55})_r$, K_{44}, and length of the beam. It is interesting to note that the induced twist is substantially reduced by constrained warping effects.

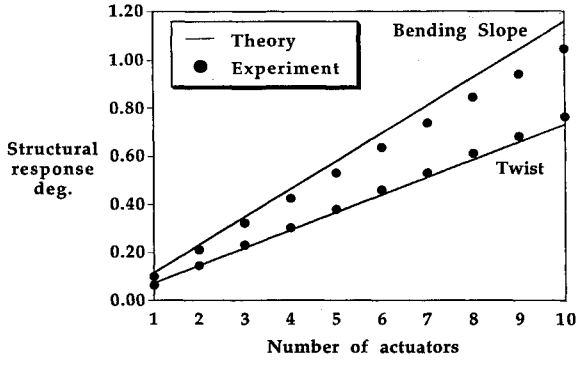

Fig. 8 Influence of number of actuators on tip structural response of graphite-epoxy bending-torsion coupled $[30]_{24}$ solid beam, applied electric field = 15 V/mil.

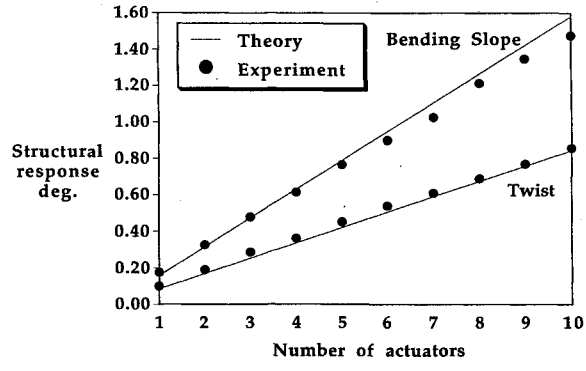

Fig. 9 Influence of number of actuators on structural response of graphite-epoxy bending-torsion coupled $[45]_{24}$ solid beam, applied electric field = 15 V/mil.

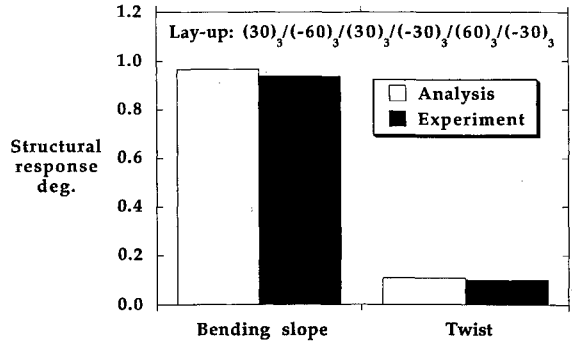

Fig. 10 Structural response of extension-torsion coupled solid beam under piezoactuation: bending due to bending actuation and twist due to extensional actuation.

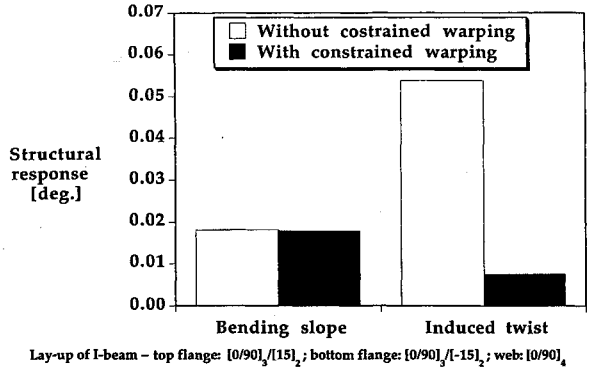

Fig. 11 Bending-torsion coupled graphite-epoxy I beam with bending piezoactuator, applied electric field = 15 V/mil.

Conclusion

Analysis of composite beams with induced-strain actuators was formulated based on Vlasov theory. Chordwise bending of a generic plate segment of beam, which is normally neglected for most beam analyses, was included to predict the structural response of bending-torsion coupled beams with induced-strain actuation. To provide the experimental correlation to the analysis, bending-torsion and extension-torsion coupled graphite-epoxy beams of solid rectangular section were fabricated using an autoclave molding technique. Piezoelectric actuation was used to apply bending moment and axial force on these beams, and the resulting bending slope and twist at the tip were measured using a laser optical system. Based on this study, the following conclusions are made:

1) For solid beams under piezoactuation, the analysis must be modified to include chordwise strain and curvature of plate segment of the beam. Chordwise bending has much more influence on the twisting than the bending of bending-torsion coupled beams under piezoelectric actuation. For $[45]_{24}$ graphite-epoxy beams, the tip twist is increased by about 110% by the chordwise actuator moment.

2) There is a significant reduction of effectiveness of induced actuation with the inclusion of copper sheeting between piezoelectric element and substructure. For $[45]_{24}$ graphite-epoxy beams, the induced tip twist is reduced by more than 50% by the copper sheet.

3) With distributed actuators, the structural response can be calculated by superposition.

4) Warping constraints influence the induced twist of bending-torsion coupled composite I-beam substantially.

Appendix: Elements of the [K] Matrix

$$K_{11} = \int_s A_{11}\, ds \qquad \text{(A1)}$$

$$K_{15} = -2\int_s B_{16}\,ds \tag{A2}$$

$$K_{22} = \int_s (A_{11}y^2 + 2B_{11}y\cos\theta + D_{11}\cos^2\theta)\,ds \tag{A3}$$

$$K_{25} = 2\int_s (B_{16}y + D_{16}\cos\theta)\,ds \tag{A4}$$

$$K_{26} = \int_s (A_{16}y + B_{16}\cos\theta)\cos\theta\,ds \tag{A5}$$

$$K_{55} = 4\int_s D_{66}\,ds \tag{A6}$$

$$K_{210} = \int_s D_{12}\ddot{\alpha}\cos\theta\,ds \tag{A7}$$

$$K_{510} = 2\int_s D_{26}\ddot{\alpha}\,ds \tag{A8}$$

$$K_{1010} = \int_s D_{22}\ddot{\alpha}\,ds \tag{A9}$$

$$K_{44} = \int_s (D_{11}q^2 + 2B_{11}q\lambda + A_{11}\lambda^2)\,ds \tag{A10}$$

For a solid rectangular section beam:

$$\lambda = 0, \quad q = s, \quad y = 0, \quad \theta = 0, \quad \alpha = s^2/2 \tag{A11}$$

Using relations (A11), relations (A1–A10) become

$$K_{11} = b_s A_{11} \tag{A12}$$

$$K_{15} = 2b_s B_{16} \tag{A13}$$

$$K_{22} = b_s D_{11} \tag{A14}$$

$$K_{25} = 2b_s D_{16} \tag{A15}$$

$$K_{26} = b_s B_{16} \tag{A16}$$

$$K_{44} = D_{11}(b_s^3/12) \tag{A17}$$

$$K_{55} = 4b_s D_{66} \tag{A18}$$

$$K_{210} = b_s D_{12} \tag{A19}$$

$$K_{510} = 2b_s D_{26} \tag{A20}$$

$$K_{1010} = b_s D_{22} \tag{A21}$$

Acknowledgment

This research work was supported by the Army Research Office under Contract DAAL-03-92-G-0121, Technical Monitor, Gary Anderson.

References

[1]Chandra, R., and Chopra, I., "Experimental and Theoretical Analysis of Composite I-Beams with Elastic Couplings," *AIAA Journal,* Vol. 29, No. 12, 1991, pp. 2197–2206.

[2]Gjelsvik, A., *The Theory of Thin-walled Beams,* Wiley, New York, 1981.

[3]Chandra, R., and Chopra, I., "Vibration Characteristics of Composite I-Beams with Elastic Couplings under Rotation," *Journal of Aircraft* (to be published).

[4]Chandra, R., and Chopra, I., "Structural Behavior of Two-Cell Composite Rotor Blades with Elastic Couplings," *AIAA Journal,* Vol. 30, No. 12, 1992, pp. 2914–2921.

[5]Chandra, R., and Chopra, I., "Structural Response of Composite Beams and Blades," *Composite Engineering,* Vol. 2, No. 5-7, 1992, pp. 347–374.

[6]Crawley, E., and de Luis, J., "Use of Piezoelectric Actuators as Elements of Intelligent Structures," *AIAA Journal,* Vol. 25, No. 10, 1987, pp. 1373–1385.

[7]Crawley, E., and Anderson, E., "Detailed Models of Piezoceramic Actuation of Beams," *Journal of Intelligent Material Systems and Structures,* Vol. 1, No. 1, 1990, pp. 4–25.

[8]Crawley, E., de Luis, J., Hagwood, N. W., and Anderson, E. H., "Development of Piezoelectric Technology for Applications in Control of Intelligent Structures," *Proceedings of the American Control Conference,* 1988, pp. 1890–1896.

[9]Crawley, E. F., and Lazarus, K.B., "Induced Strain Actuation of Isotropic and Anisotropic Plates," *AIAA Journal,* Vol. 29, No. 6, 1991, pp. 944–951.

[10]Im, S., and Atluri, S. N., "Effects of a Piezo-Actuator on a Finitely Deformed Beam Subjected to General Loading," *AIAA Journal,* Vol. 27, No. 12, 1989, pp. 1801–1807.

[11]Robbins, D. H., and Reddy, J. N., "Analysis of Piezoelectrically Actuated Beams using a Layer-wise Displacement Theory," *Computers and Structures,* Vol. 41, No. 2, 1991, pp. 265–279.

[12]Jensen, D. W., and Crawley, E. F., "Frequency Determination Techniques for Cantilevered Plates with Bending-Torsion Coupling," *AIAA Journal,* Vol. 22, No. 3, 1984, pp. 415–420.

[13]Chandra, R., and Chopra, I., "Structural Modeling of Composite Beams with Induced Strain Actuators," *Proceedings of the Winter Annual Meeting of the American Society of Mechanical Engineers,* Anaheim, CA, Nov. 1992.

[14]Winckler, S. J., "Hygrothermally Curvature Stable Laminates with Tension-Torsion Coupling," *Journal of the American Helicopter Society,* Vol. 30, No. 3, 1985, pp. 56–58.